Ballistic and thermalized regimes to tune structure and conducting properties of W-Mo thin films

Houssem Boukhalfa, Valérie Potin, Nicolas Martin

Journal Pre-proof

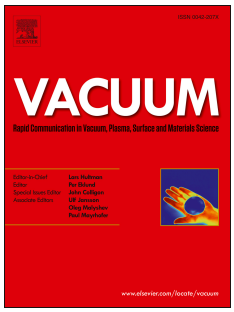

Ballistic and thermalized regimes to tune structure and conducting properties of W–Mo thin films

Houssem Boukhalfa, Valérie Potin, Nicolas Martin

PII: S0042-207X(22)00469-9

DOI: https://doi.org/10.1016/j.vacuum.2022.111347

Reference: VAC 111347

To appear in: *Vacuum*

Received Date: 16 May 2022

Revised Date: 15 July 2022

Accepted Date: 16 July 2022

Please cite this article as: Boukhalfa H, Potin Valé, Martin N, Ballistic and thermalized regimes to tune structure and conducting properties of W–Mo thin films, *Vacuum* (2022), doi: https://doi.org/10.1016/j.vacuum.2022.111347.

Ballistic and thermalized regimes to tune structure and conducting properties of W-Mo thin films

Houssem Boukhalfa [1], Valérie Potin [1] and Nicolas Martin [2 *]

[1]Laboratoire Interdisciplinaire Carnot de Bourgogne (ICB), UMR 6303 CNRS Université Bourgogne Franche-Comté, 9, Avenue Alain Savary, BP 47 870, F-21078 Dijon Cedex, France

[2]Institut FEMTO-ST, UMR 6174 CNRS Université Bourgogne Franche-Comté, 15B, Avenue des montboucons, 25030 Besançon Cedex, France

* Corresponding author: nicolas.martin@femto-st.fr

Highlights

- W-Mo nanorod films fabricated by co-sputtering with the GLAD technique.
- Ballistic and thermalized regimes tune the columnar architecture.
- Anisotropic to cauliflower structures are produced as pressure rises.
- W-Mo films resistivity follows a rule of mixtures or a corrected Nordheim's law.

Graphical abstract

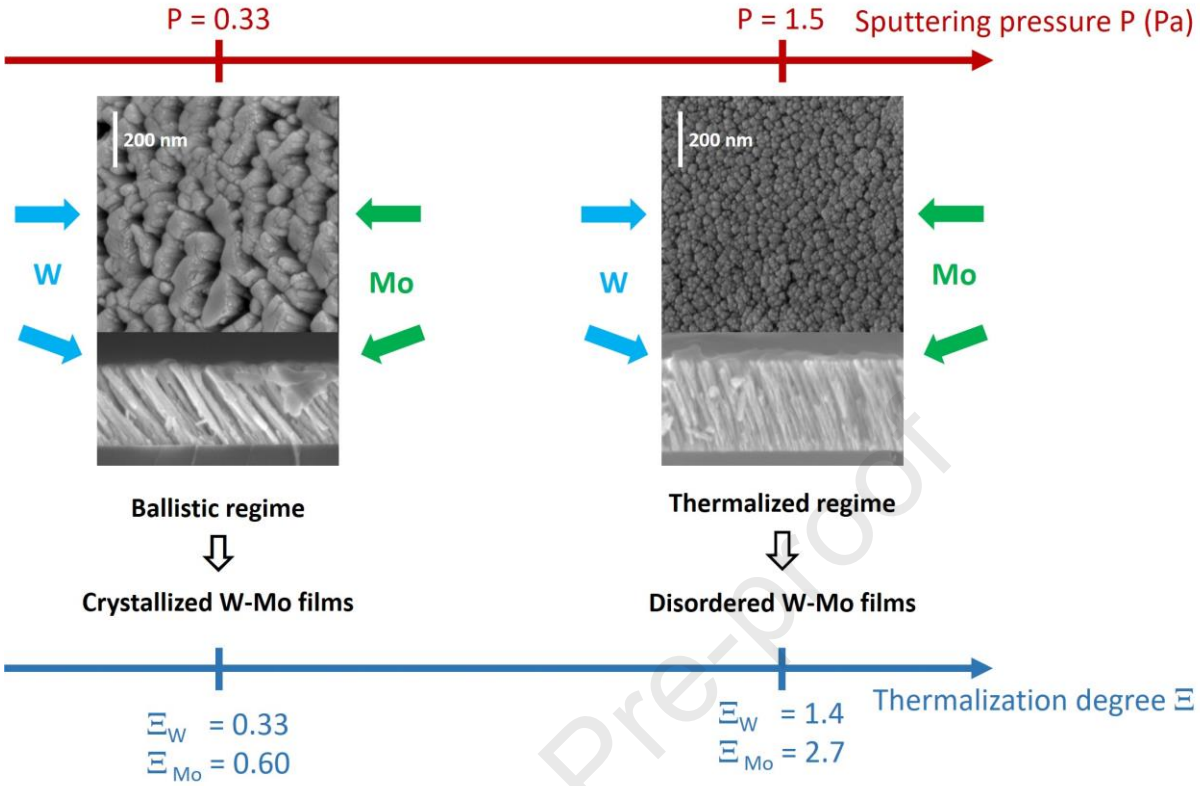

Abstract

W-Mo thin films are prepared by magnetron co-sputtering using glancing angle deposition. The same deposition angle $\alpha_W = \alpha_{Mo} = 80°$ is used for both W and Mo targets. Two different sputtering pressures are used: 0.33 Pa and 1.5 Pa, which correspond to ballistic and thermalized regimes of sputtered atoms, respectively. For each regime, W target current is kept at $I_W = 140$ mA, whereas Mo target current gradually changes from $I_{Mo} = 10$ to 200 mA. Both regimes present porous thin films with inclined columns due to the shadowing effect that characterizes the films prepared with high oblique angle. Surface and cross-section morphologies exhibit elliptically bounded columns for the ballistic regime while they change to a cauliflower-like structure as thermalization prevails. At low pressure, the column angle β decreases with Mo target current and a Mo-enrichment of the films is noticed. Films are poorly crystallized at high pressure whatever the Mo target current with a high resistive behavior. The electrical resistivity *vs.* Mo content follows a rule of mixtures for films prepared at low pressure, whereas these deposited at high pressure correlate with a corrected Nordheim's law.

Keywords

Thin films, co-sputtering, ballistic particles, thermalization, columns, electrical resistivity

Introduction

Thin films are materials defined by a low thickness comprised between a few nanometers and several micrometers. Thin films production has begun during the Antiquity and more precisely during the middle bronze age (more than 5000 years ago [1]). Indeed, Egyptians produced gold thin films characterized by a thickness below 300 nm and used them for decoration and optics. Since this period, different civilizations contributed to thin films production in term of techniques and materials. However, the important development on thin films took place at the end of 1700s and in the early 1800s with the development of vacuum technology, scientists being focused on the investigation of thin films properties and on their growth behavior. Films were prepared by electrodeposition on copper using voltaic pile, antireflective coatings were deposited on glass telescope lenses using concentrated sulfuric acid and vanadium pentoxide films were obtained using sol-gel technique. Afterwards, iron oxide thin films were sputter deposited on silver substrate [1]. The continuous development carried out on thin films production from centuries until these days opened the doors to use them in different industrial domains and applications such as electronics, nanotechnology, sensors, etc. [2].

Thin films development is related to the improvement of deposition techniques helping to create innovative films with higher performances. Nowadays, among the different elaboration methods for thin films production, we focus on DC magnetron sputtering physical vapor deposition (PVD) combined with the glancing angle co-deposition technique. This deposition technique is based on the same working principles as GLAD (GLancing Angle Deposition) technique with the use of several targets instead of only one. Basically, GLAD technique [3] allows modifying the films structure and density by inclining the target with respect to the substrate (deposition angle α). Thin films porosity increases with deposition angle, leading to an increase of the specific surface, particularly interesting for applications

such as catalysis or gas sensors [4, 5]. Three-dimensional Ta-Si thin films were grown on silica spheres with the GLAD co-sputtering technique using two opposite Ta and Si targets. Deposition was performed simultaneously or sequentially leading to laterally or vertically separated Ta and Si components [6, 7]. Simultaneous co-deposition with two different targets was also performed for W-Cu [8], W-Ag [9], Ti-Ag [10], NiWO [11] and so on.

Films structure and properties highly depend on the operating parameters as the deposited materials themselves, the current applied to each target, the target-to-substrate distance, the inert gas nature or the pressure. This latter appears to be a key deposition parameter that influences the structure and therefore the properties of co-deposited thin films as shown for W-Cu [12]. Indeed, the pressure variation from low values to high ones induces a switchover between two different regimes during films deposition. The ballistic and thermalized regimes characterize the films deposited at low and high pressure, respectively [10, 13, 14]. The mean free path λ of sputtered particles depends on the sputtering gas pressure imposed during the film deposition. For low λ values (e.g., below a few mm), the sputtered particles undergo numerous collisions leading to a thermalized regime (diffusive behavior) characterized by a loss of kinetic energy and directionality. Due to collisions with inert gas atoms (e.g., argon), sputtered particles become thermalized with a kinetic energy in the order of 1 eV. In contrast, for high λ values (higher than several cm), the ballistic regime corresponds to a few collisions inducing more energetic and directional particles. Between the high and low pressures, both ballistic and thermalized regimes coexist. The calculation of the thermalization degree helps to determine the balance between ballistic and thermalized regimes [13]. Indeed, low (< 1) and high (> 1) thermalization degrees correspond to ballistic and thermalized regimes, respectively. For GLAD thin films, the thermalization degree has been calculated to determine the type of regime of sputtered atoms and their effect on the different films properties as Au [13], Ti [14], TiO_2 [15], W [16] while for co-deposited thin films, a qualitative approach was mainly performed

[12, 17]. It is also worth noticing that theoretical and experimental studies about the GLAD process involving a single source of atoms prosper in the literature for the last ten years. However, investigations reporting the GLAD co-deposition process with at least two sources begin to be significant with an experimental approach remaining as the most pragmatic method.

In this paper, we study W-Mo thin films prepared by DC magnetron co-sputtering using GLAD technique with two different W and Mo targets. Structural and electrical properties of thin films strongly depend on many deposition parameters. For our study, the sputtering pressure is a key parameter since it allows playing with the direction and the energy of the sputtered particles, and so understanding the role of regimes (ballistic or thermalized) on the final structure of GLAD co-deposited W-Mo films. Using two different targets, varying the current intensity applied on one of them can also have an impact on films microstructure and composition. Other parameters such as deposition angles, distances between the substrate and the targets and the current intensity applied on tungsten target are fixed. Only two parameters are modified, the argon pressure with a low- and a high-pressure value (0.33 Pa and 1.5 Pa corresponding to the ballistic and thermalized regimes, respectively) and the current intensity applied on molybdenum target that varies from 10 to 200 mA. The effect of these two opposite sputtering pressures and Mo current intensity on the morphology, crystallography and electrical resistivity of W-Mo thin films is studied and discussed.

Experimental details

W-Mo thin films are deposited at room temperature on glass and silicon substrates by DC magnetron sputtering using two opposite metallic targets (51 mm of diameter and 99.9% purity): tungsten and molybdenum. They are located inside a 40 L homemade vacuum chamber pumped down to a pressure below 10^{-5} Pa. The distance between W and Mo target centers and the substrate are fixed to 65 mm and 95 mm, respectively. W and Mo targets are inclined with

the same oblique angle α = 80°, corresponding to the angle between the substrate normal and the target normal. This deposition configuration is the same as for W-Ag thin films deposition [9]. Thin films are deposited in a pure argon atmosphere with two different flow rates of 4.4 and 20 sccm, corresponding to sputtering pressures of 0.33 and 1.5 Pa, respectively. All substrates are cleaned with acetone and ethanol before deposition. For both pressures, W-Mo thin films are prepared using a fixed W target current I_W = 140 mA and various Mo target currents I_{Mo} between 10 and 200 mA. Deposition times are adjusted to get a 300 nm film thickness whatever the Mo target current and pressure. Table 1 summarizes operating conditions for both sputtering pressures.

Pressure P (± 0.01 Pa)	Mo target current I_{Mo} (±1 mA)	10	20	30	50	100	150	200
0.33	W target voltage U_W (±3 V)	264	263	262	283	274	272	271
	Mo target voltage U_{Mo} (±3 V)	257	254	258	290	295	303	314
	Deposition rate (±30 nm h^{-1})	430	500	500	510	560	670	680
	Column angle β (±2°)	36	35	34	29	20	10	4
1.50	W target voltage U_W (±3 V)	279	280	282	281	279	281	281
	Mo target voltage U_{Mo} (±3 V)	193	201	208	220	238	250	258
	Deposition rate (±30 nm h^{-1})	750	790	820	840	910	1070	1180
	Column angle β (±2°)	17	18	17	16	14	9	8

Table 1: Deposition parameters of W-Mo thin films at low (0.33 Pa) and high (1.5 Pa) pressure.

Structural analyzes are carried out on the films deposited on silicon substrates. Thin films morphology is studied from top and cross-section views using JEOL JSM 7600F and Hitachi SU8230 scanning electron microscopes. Energy dispersive X-ray spectrometry (EDX)

attached to SEM is used during surface observations to determine the atomic concentration of W and Mo for all films. The crystallographic structure is characterized by X-ray diffraction (XRD) technique using a Bruker D8 focus diffractometer with a copper X-ray tube (Cu $\lambda_{K\alpha}$ = 0.15419 nm) with a Bragg-Brentano configuration. Scans are recorded with 2θ from 20° to 120° with a step of a 0.02° per 1s. Electrical resistivity is measured at room temperature using the four-probe van der Pauw method for films deposited on glass. The electrical anisotropy [18] defined as the ratio between electrical resistivity measured following perpendicular and parallel directions to the sputtered particle fluxes is also determined.

Results and discussion

It is well know that the transport mechanisms of sputtered particles between substrate and target can affect the films growth. Alvarez *et al.* [14] defined a key parameter, namely the thermalization degree Ξ (dimensionless), as a function of the sputtering pressure P (Pa) and the target-to-substrate distance L (m), following:

$$\Xi = C \times P \times L \quad (1)$$

Where C is a constant depending on the geometrical cross-section for an elastic collision between a sputtered and a gas atom, the gas temperature, and the number of elastic collisions required for thermalization of a sputtered atom. This number of elastic collisions η is determined from the following relationship proposed by Westwood [19]:

$$\eta = \frac{ln\left(\frac{v_g}{v_0}\right)}{ln\left(\frac{v_t}{v}\right)} \quad (2)$$

It represents the number of collisions needed to reduce the initial velocity v_0 (m s^{-1}) of a sputtered atom to the thermal velocity v_g (m s^{-1}). The ratio v_t/v depends on masses of gas and sputtered atom (velocity of such sputtered atom changing from v to v_t in the direction of v after

the collision). Taking a gas temperature of 300 K and an ejection energy of 5 eV for sputtered atoms, calculations give η = 9 and 5 for W and Mo, respectively.

For a thermalization degree Ξ < 1, the transport behavior of sputtered atoms mainly follows a ballistic regime, whereas a thermalized regime is considered for Ξ > 1. On the other hand, the flux Φ_B of ballistic sputtered atoms can be determined *vs.* thermalization degree from:

$$\Phi_B = \Phi_0 \times \frac{1-e^{-\Xi}}{\Xi} \quad (3)$$

Where Φ_0 is the flux of sputtered atoms at the target (arb. units), and thus for a given deposition angle α, it becomes:

$$\Phi_B(\alpha) = \Phi_0 \times e^{-\Xi} \times cos(\alpha) \quad (4)$$

Assuming a deposition angle α = 80° for both targets, the target-to-substrate distances (65 mm and 95 mm for W and Mo, respectively), a gas temperature T = 300 K, and considering the number of elastic collisions required for thermalization for W and Mo atoms as η = 9 and 5, respectively, ballistic and thermalized proportions can be calculated as a function of the sputtering pressure for a deposition angle α = 80° (Fig. 1a) and for conventional sputtering, i.e. α = 0° (Fig. 1b).

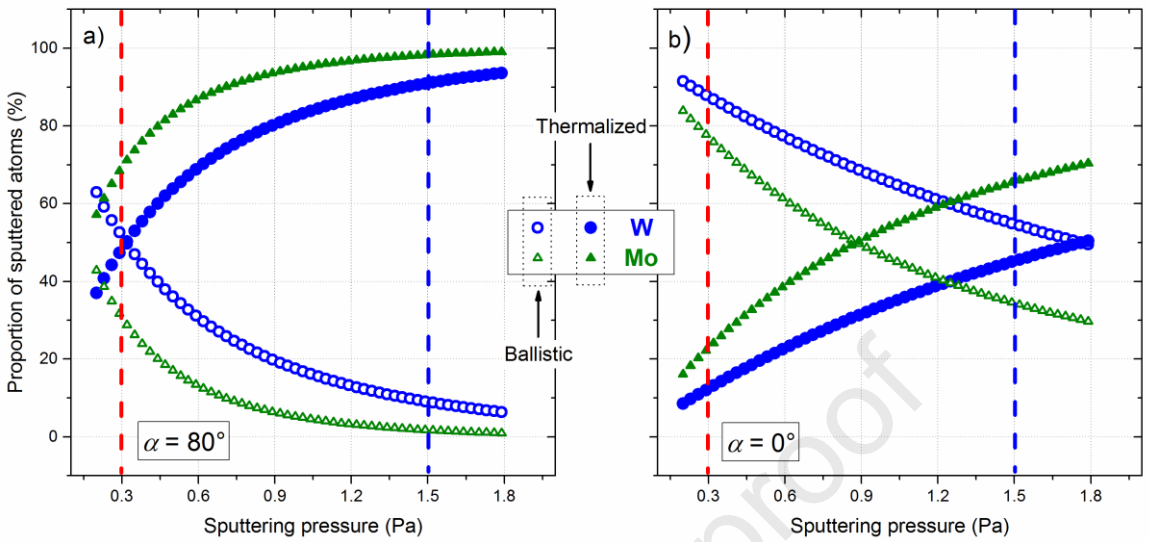

Figure 1: Proportion of thermalized (fill symbols) and ballistic (open symbols) W and Mo sputtered atoms *vs.* sputtering pressure calculated for a deposition angle: a) $\alpha = 80°$ and b) $\alpha = 0°$ (conventional sputtering). Red and blue dashed lines correspond to sputtering pressures of 0.33 and 1.5 Pa, respectively.

For $\alpha = 80°$, both metals experience a rapid thermalization effect as the sputtering pressure rises from 0.33 to 1.5 Pa. It is also worth noting that the thermalization degree for W (Mo) increases from $\Xi = 0.3$ (0.6) to 1.4 (2.7) as the sputtering pressure changes from 0.33 to 1.5 Pa. For the lowest sputtering pressure (0.33 Pa), the proportion of ballistic W atoms is 49% (28% for Mo) and abruptly drops to 9.0% (1.7%) at 1.5 Pa. As a result, most of the W and Mo sputtered atoms are thermalized by the Ar background gas for the highest sputtering pressure, whereas a ballistic regime balances with the thermalized one at 0.33 Pa. These results well agree with investigations previously reported by Garcia-Martin *et al.* [15]. Self-shadowing

mechanisms and collisional processes of sputtered particles (especially thermalization degree) have to be considered to discuss morphology and inclination of the resulting nanocolumns. Thermalization effect becomes less significant when films are deposited by conventional sputtering with $\alpha = 0°$ (Fig. 1b). At low sputtering pressure (0.33 Pa), the ballistic regime is predominant for W as well as Mo atoms. The influence of atomic mass is clearly illustrated at high pressure (1.5 Pa) since more than half part of W atoms remain in the ballistic regime, whereas majority of Mo atoms (about 65%) are thermalized.

Pedrosa *et al.* [20] studied Ti thin films with different argon pressures and showed that when $\Xi < 1$, the incident particles present some high energy and directivity, the contribution being mainly ballistic. Rising the argon sputtering pressure leads to an increase of the thermalization degree Ξ, which favors the biased diffusion contribution while the kinetic energy-induced mobility process decreases due to the enhanced thermalization of the particles with pressure. The sputtered particles become less directional and also less energetic as Ξ increases.

Figure 2 shows the deposition rate of W-Mo thin films produced with two different argon pressures (0.33 and 1.5 Pa), with a fixed W target current of 140 mA and various Mo target currents between 10 and 200 mA.

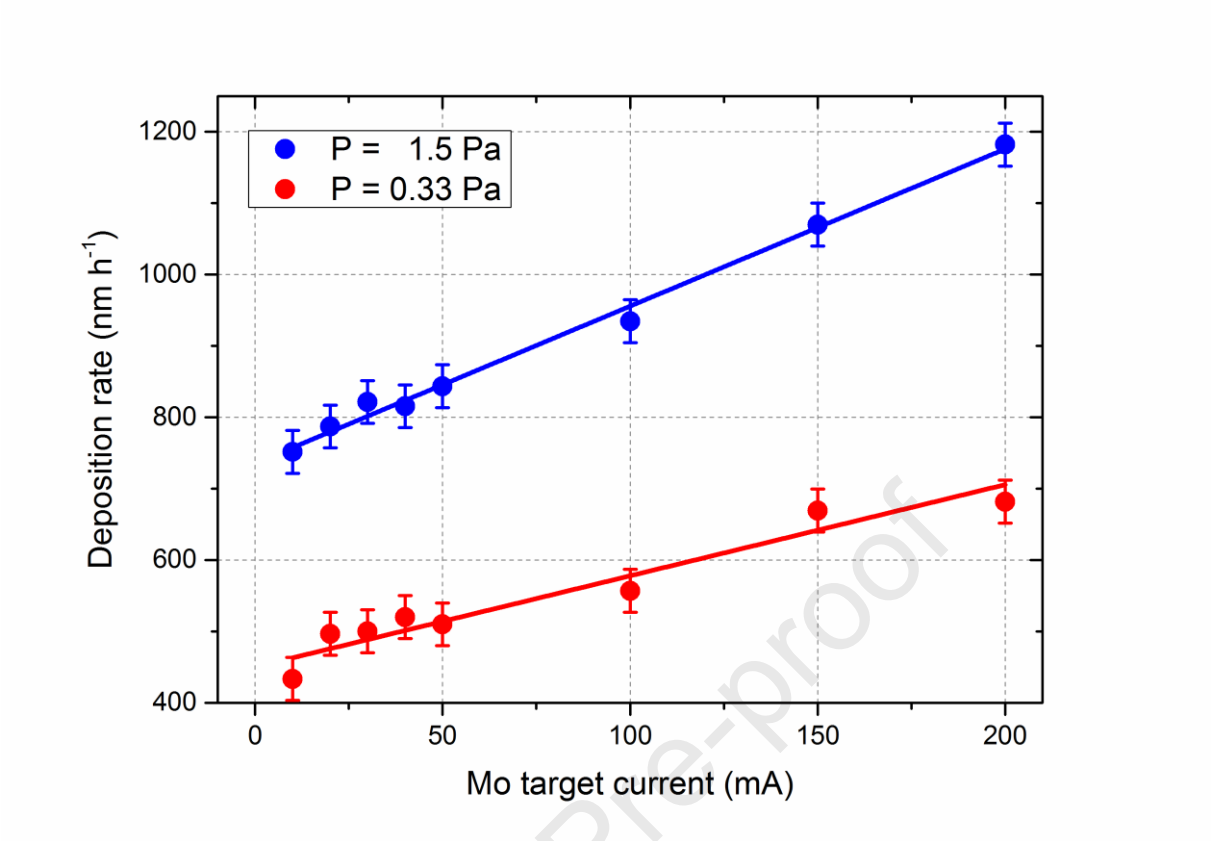

Figure 2: Deposition rate as a function of the Mo target current and for two argon sputtering pressures: 0.33 and 1.5 Pa.

The deposition rate corresponds to the thickness of the films measured by profilometry divided by the deposition time. For both pressures, the deposition rate presents a linear evolution *vs.* Mo target current. As I_{Mo} changes from 10 to 200 mA, it increases from 433 to 681nmh^{-1} at low pressure with a slope of 1.3 nmh^{-1}mA^{-1} while it varies from 751 to 1182 nmh^{-1} at high pressure with a slope of 2.2 nmh^{-1}mA^{-1}. The increase of the deposition rate with Mo target current is linked to the similar increase of the Mo target voltage (Table 1). The latter being connected to the argon ions impinging on the target, it enhances the sputtering yield and thus the amount of Mo atoms on the substrate. The deposition rate evolution with target current variation was also studied for co-deposited thin films with the GLAD technique. For W-Cu thin films [12], it was reported that the modification of both W and Cu current intensities affects the

deposition rate of the whole film. For co-sputtering, each target presents its own deposition rate that is related to the current intensity applied on it and the deposition rate of the whole film is a combination between these two deposition rates.

Despite a similar linear behavior with Mo target current for both argon pressures, the deposition rate presents higher values at high pressure than at low pressure implementing the same sputtering conditions (target-to-substrate distances, Mo and W current intensities). Deposition rate of metallic thin films deposited by conventional sputtering ($\alpha = 0°$) obviously depends on the pressure. Trend varies as a function of the nature of the sputtered material, especially his weight compared to that of the plasma gas [21]. The increase of deposition rate is greatest for the sputtered material with highest atomic weight, which is mainly connected to the relative mass of the sputtered atom compared with the gas atom. The greater the relative mass of the sputtered atom, the greater the deposition rate is at high pressure (persistence of the initial direction of travel towards the substrate). This persistence is well illustrated in figure 1b where W atoms (heavier than Mo) keep a significant ballistic character at high pressure (1.5 Pa), whereas Mo atoms become more thermalized. At first, deposition rate can be considered as the mixture between the highly directed and energetic ballistic contribution and the thermalized contribution characterized by an energy loss of the atoms and their random movements in the plasma gas [14]. When the pressure increases, the concentration of argon atoms also increases inducing more collisions with the W and Mo particles. At high pressure (1.5 Pa), the effect of thermalization is even more marked by GLAD with $\alpha = 80°$ (Fig. 1a). As a result, this higher deposition rate measured as pressure rises is mainly assigned to the enhanced proportion of thermalized atoms (W and Mo) impinging on the growing film (such a proportion being particularly favored for high deposition angle).

W-Mo thin films are examined by scanning electron microscopy (SEM) to reveal the effect of pressure and Mo target current variations on their morphology. Figures 3 and 4 show

surface and cross section observations of three different W-Mo thin films (with I_{Mo} = 10, 40 and 150 mA) and for both pressures. SEM views are only displayed from the center of the substrate holder as similar morphologies are pointed out along the specimen whole length except at the extremities.

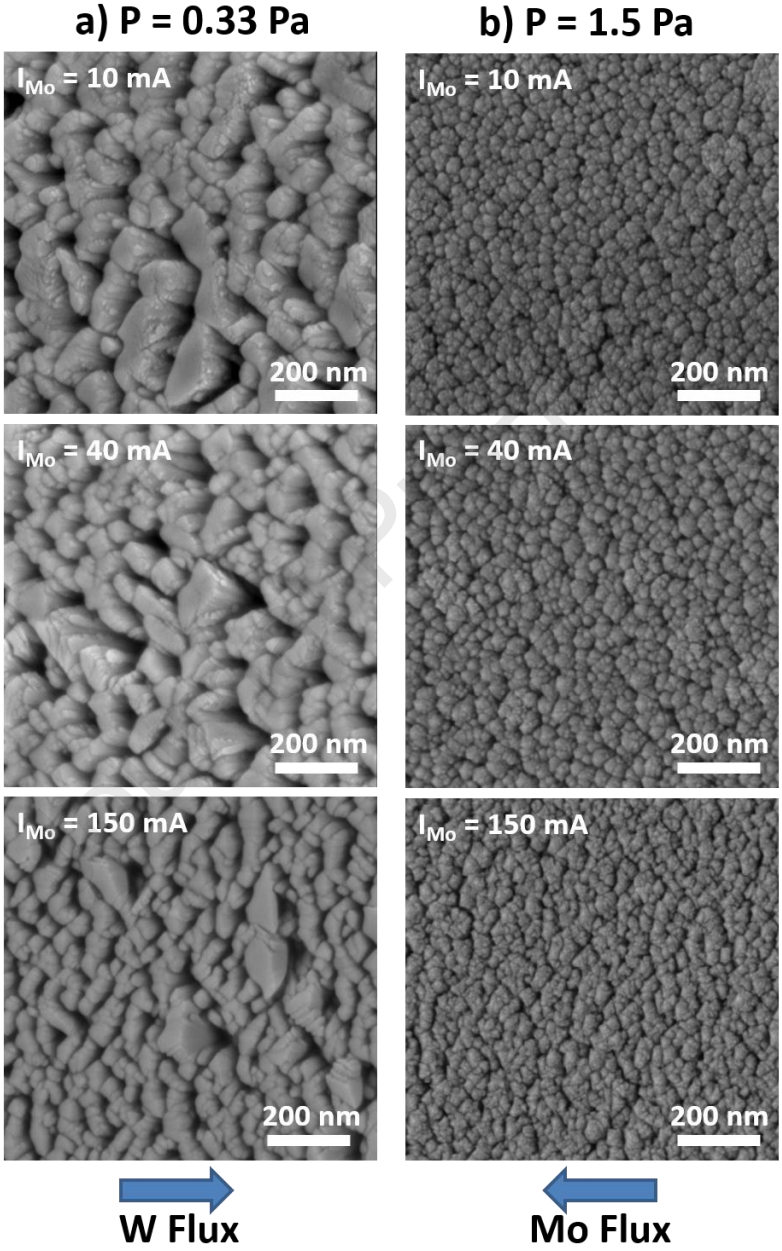

Figure 3: Top observations by SEM of W-Mo thin films deposited with a sputtering pressure of: a) 0.33 Pa and b) 1.5 Pa. A fixed W target current (I_W = 140 mA) and various Mo target currents from 10 to 150 mA are used.

All studied films prepared with different sputtering conditions present a columnar aspect with important voids and well separated and inclined columns. This films morphology is highly related to the self-shadowing effect [22] that is especially present in GLAD films and enhanced for high deposition angle α. Surface observations point out two different surface morphologies due to argon sputtering pressure variations. At low pressure, an asymmetric morphology of the columns (elliptical structure) is observed with a lateral connection between them in the direction perpendicular to the particle fluxes. This asymmetric microstructure is related to the self-shadowing effect, the connection of the columns being favored in the direction perpendicular to the particle fluxes [23, 24]. This anisotropic behavior has been previously reported for different GLAD thin films based on W or Mo (using only one metallic target) [25, 26] but also for co-deposited ones as W-Cu [12]. Based-on the top observations by SEM of W-Mo films (Fig. 3a) and with a simple image analysis as suggested by El Beainou *et al.* [27], the effective widths of the columns (parallel and perpendicular to the particle fluxes) can be obtained as a first approximation. For W-Mo films prepared with the lowest I_{Mo} = 10 mA, the average column width parallel to the fluxes is overs 200 nm against 40 nm for the perpendicular one, giving rise to a column width ratio of 5. This order of magnitude agrees with those reported for single or bimetallic films fabricated with similar operating conditions [27]. An increase of the Mo target current (I_{Mo} = 150 mA) disturbs the columnar W growth (Mo enrichment as shown later in Fig. 5 and occurrence of different phases with clear W/Mo interfaces as shown in the Supplementary Material). The column apex exhibits a less elliptical shape and becomes smaller in both directions (parallel and perpendicular to the particle fluxes) with a column width ratio reducing to about 2.

At high pressure, surface morphology changes and becomes less anisotropic presenting a cauliflower-like structure. Smaller columns are formed compared to low pressure ones and

columns are agglomerated with a circular form unlike the elliptical structure obtained at low pressure (top column diameter is lower than 50 nm, neglecting the bundling phenomenon as typically observed in Fig. 3b whatever the Mo target current). Lateral growth is restrained since impinging particles on the growing film do not originate from 2 clear directions (W and Mo targets) but fluxes rather exhibit a multidirectional character due to the thermalized regime reached at this high pressure.

The observed difference of morphology is linked to the more or less ballistic character of W and Mo particles inside the vacuum chamber, and more precisely to the number of collisions experienced by the particles, and so to the proportion of ballistic and thermalized atoms in the zone between the substrate and the targets, as shown in figure 1. At low pressure, the sputtered particles (W and Mo) cross the path between the targets and the substrate with only a few interactions with argon atoms due to their low density. Therefore, the particles trajectory appears to be highly directional. In contrast, when the argon sputtering pressure increases to 1.5 Pa, the argon density also increases as well as interactions between them and the sputtered particles, affecting their mean free path λ that strongly decreases (about a few mm at 1.5 Pa). With a decrease of λ, sputtered atoms are less energetic and their trajectory are less directional compared to their behavior at low pressure. Therefore, a random deposition is brought to the fore at high pressure. At certain pressure and thermalization degree ($\Xi < 1$), it was previously shown that Ti thin films lose their columnar aspect due to the absence of particle directionality [28].

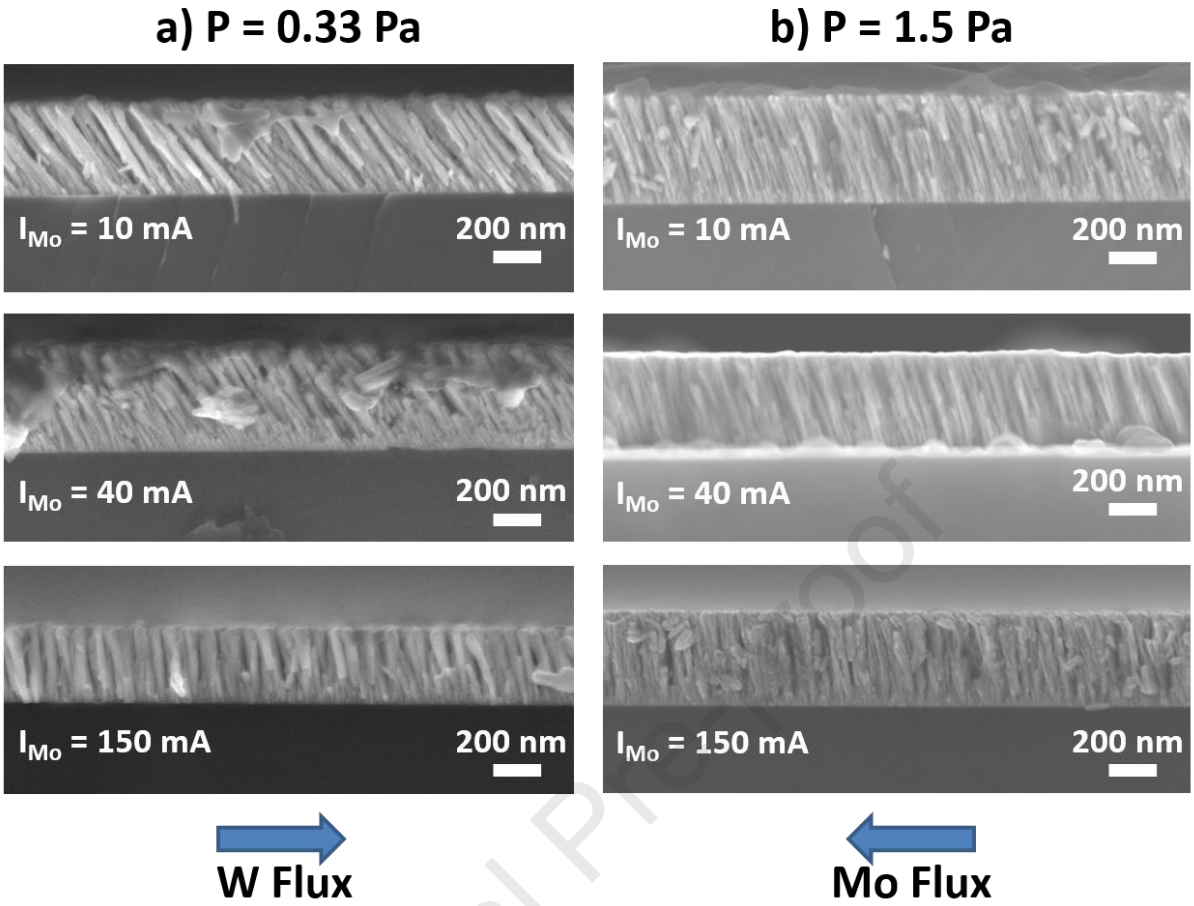

Figure 4: Cross-section observations by SEM of W-Mo thin films prepared with an argon pressure equal to a) 0.33 Pa and b) 1.5 Pa, and with a fixed W target current (I_W = 140 mA) and various Mo target currents from 10 to 150 mA.

A columnar structure is conserved for all samples despite Mo target current and pressure variations. Moreover, columns are inclined towards W target as shown in Fig. 4. Voids between the columns are also observed, which are related to the self-shadowing effect induced by the targets inclination and becoming more and more significant for higher oblique angles [22]. Pressure variation affects the films morphology and mainly the columnar tilt angle β, defined as the angle between the normal to the substrate surface and the inclined columns direction. Columns inclination can be modified by varying sputtering parameters such as Mo target current and pressure until obtaining straightened ones (Table 1). At lower pressure, columnar

tilt angle β presents a higher value for the low Mo target current (β = 36°), that reduce as I_{Mo} increases until reaching practically vertical columns (β = 4°). At high pressure, the columnar tilt angle β presents lower values for the lowest I_{Mo} (β = 18°). If a straighten growth of the columns is still pointed out with I_{Mo}, it is clearly less pronounced as the β angle (β = 8°) does not reach the values obtained at low pressure. This columnar aspect with inclined columns has been reported for W films [25] with similar deposition conditions (pressure = 0.25 Pa, angle α = 80°, target-to-substrate distance = 65 mm) while a columnar aspect has also been obtained for Mo films produced at low pressure (0.08 Pa) [29].

The evolution of W-Mo thin films morphology can be discussed considering the morphology of W and Mo thin films deposited alone as well as the surface mobility of these particles. Particles mobility is based on the self-diffusion length as calculated previously [9]. W and Mo particles present nearly the same surface diffusion activation energy E_d (equal to 1.22 and 1.20 eV, respectively [30]) and thus a similar mobility. Therefore, a real columnar growth competition occurs between W and Mo, depending on the dominance of W or Mo flux. This dominance is related to several factors, the Mo target current variation being the first one as W target current is fixed. A second factor having a possible impact on the dominating flux, is the sputtering yield. However, this impact is limited as values are practically similar for W (around 0.290 for an Ar^+ energy of 275 eV) and Mo (around 0.296 for an Ar^+ energy of 250 eV). The vacuum chamber geometry is also one of the important parameters to consider as the distance between the target and the substrate affects the deposition rate of each element, directly impacting the flux predominance. W and Mo target-to-substrate distances are different, being equal to 65 and 95 mm, respectively. So, to compensate the difference between these distances, the equilibrium between the fluxes can only be reached for a Mo target current higher than 140 mA (value of W target current). Taking into account all these factors, the column angle β decreases with I_{Mo} until the columns are perpendicular to the substrate. Columns would be

oriented toward the Mo target if the Mo flux becomes dominant. This relation between the particle fluxes from two targets and the columns inclination has previously been verified for W-W thin films [24].

The columnar tilt angle β is also affected by the argon sputtering pressure. Despite the decrease of β angle with Mo target current for both pressures, the impact of I_{Mo} increase is not the same. The columnar tilt angle β presents a higher gap of variation between low and high current for the films prepared at low pressure compared to those prepared at high pressure (Table 1). This difference of β angle evolution is related to the particles trajectory that becomes less directional at high pressure due to a less ballistic contribution in favor of a thermalized regime. At high pressure, the particle energy presents lower values compared to those at low pressure and lose their high directionality. The particle thermalization decreases the influence of the target current on the columns angle evolution [13]. Some studies reported a similar effect of the pressure on the columns inclination as for W [25] or Ti thin films [20], with columns being more inclined at low pressure than at high pressure. This is related to the random growth of the columns at high pressure due to the absence of the particles directionality, which leads to a less influence of Mo target current.

W-Mo atomic concentration ratio is determined using SEM-EDX with measurements at the center of the samples. It is important to note that Oxygen has been systematically detected in W-Mo films. Since EDX measurements have been performed ex-situ, and thus oxidation of thin films during elaboration and/or after it cannot be discriminated. In addition, no clear trends could be deduced from such measurements as a function of the sputtering pressure or Mo target current, leading to neglect the oxygen effect as a first approximation. The atomic concentration ratio [W]/[Mo] is strongly influenced by both sputtering parameters: pressure and Mo target current I_{Mo}, as shown in Fig. 5.

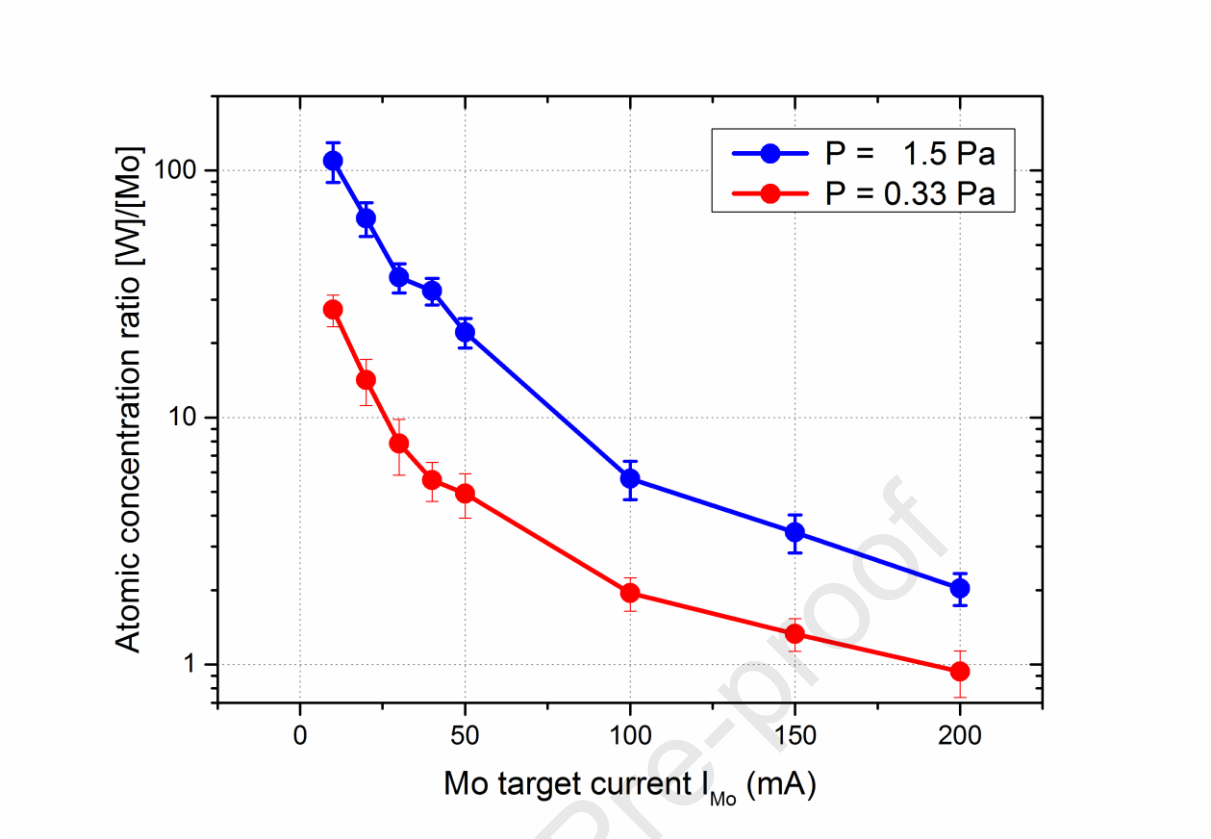

Figure 5: Atomic concentration ratio [W]/[Mo] as a function of the Mo target current for investigated sputtering pressures: 0.33 and 1.5 Pa (red and blue lines are a guide for the eye).

With a fixed W target current (I_W = 140 mA) and for all samples, I_{Mo} increase reduces the atomic concentration ratio [W]/[Mo] for both pressures. The [W]/[Mo] ratio evolution can be divided into two parts, i.e., below I_{Mo} = 50 mA and higher. The films produced with I_{Mo} = 10 mA present the highest ratio for each sample series with values close to 27 and 109 for 0.33 and 1.5 Pa, respectively. This high ratio difference between low and high pressures is significant for low I_{Mo} currents. An important ratio difference is still present at I_{Mo} = 50 mA with values close to 5 and 22 for 0.33 and 1.5 Pa, respectively. The second part of the ratio evolution corresponds to the I_{Mo} current values higher than 50 mA, for which the pressure impact becomes minimized compared to low currents. Increasing I_{Mo} and for both pressures, W and Mo concentrations tend to be the same with a ratio value becoming close to 1. For the highest Mo

target current and at 0.33 Pa, the ratio is slightly below 1, indicating that similar amounts of W and Mo have been deposited. In contrast, the samples prepared with the lowest I_{Mo} current present of course the highest ratio, corresponding to a relative W concentration of the samples above 90 at.%. It means that the films deposited at low I_{Mo} currents are practically only composed of W. This can be linked to the dominance of W atoms flux due to high I_W value compared to I_{Mo} one as well as to the distances between the substrate, and W and Mo targets equal to 65 and 95 mm, respectively. The difference of ratio between low and high pressures is related to the higher number of collisions experienced by Mo particles compared to W ones. Indeed, collisions between sputtered particles and argon gas increase with pressure but a more important distance is traveled by Mo particles as the Mo target distance is longer than W one. These collisions change the Mo particles trajectory and lead to less Mo atoms deposited on the growing film. Another factor that can be taken into account is the atomic mass as it can affect the particles trajectory during collisions. W is characterized by a higher atomic mass compared to Mo (184 and 96 amu, respectively). Therefore, W particle flux prevails over that of Mo despite pressure changes, which promotes W deposition and so a higher [W]/[Mo] ratio at high pressure.

XRD analyses are carried out on W-Mo thin films to study the evolution of the crystallographic structure with Mo target current and argon sputtering pressure variations. A clear difference on thin films crystallization is recorded, as shown in Fig. 6.

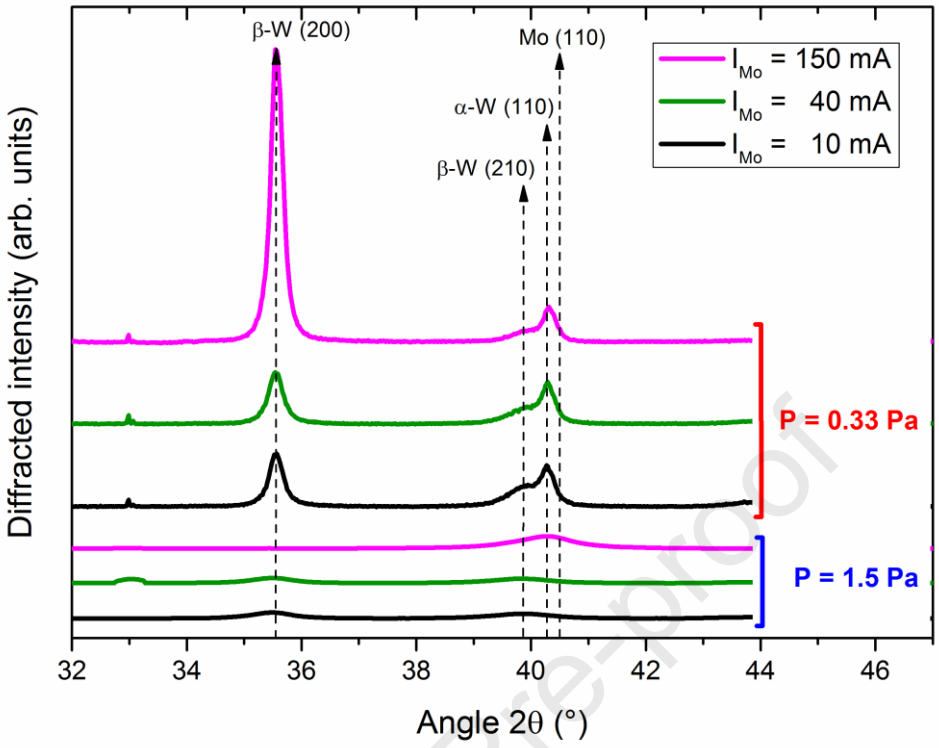

Figure 6: XRD patterns recorded in Bragg - Brentano configuration between 2θ = 32° and 47° for W-Mo thin films prepared by GLAD co-sputtering with various Mo target currents at low (0.33 Pa) and high (1.5 Pa) sputtering pressures.

Well-defined and intense peaks are recorded at low pressure (0.33 Pa) while diffracted signals at high pressure (1.5 Pa) are broad and weak. Different peaks are detected with similar 2θ values for both pressures corresponding to two different W phases. The first peak is detected at a position 2θ close to 35.5° and corresponds to the (200) planes of the metastable A15 β-W phase (ICDD-pdf # 00-047-1319). The second signal detected at 2θ = 39.5°-40.5° presents an asymmetric behavior with a larger width compared to the first peak. This is related to the presence of two peaks at very close positions attributed to different W phases. They correspond to the (210) planes of β-W phase for the first peak and (110) planes of the body-centered cubic (bcc) α-W phase (ICDD-pdf # 00-004-0806), for the second one. At low pressure, the diffracted

signal corresponding to the β-W (200) peak becomes more important as the Mo target current increases, while the second diffracted signal remains constant. These results show the predominance of the β-W phase with a preferential orientation along the (200) planes. Furthermore, a small shift of the (110) peak to higher values is detected with an I_{Mo} increase. At low current, the (110) peak corresponds to the α-W phase due to the weak amount of Mo, as previously shown with SEM-EDX analysis (Fig. 5). It is detected at the position 2θ = 40.27° while at high current this peak is shifted to the position 2θ = 40.32° (the theoretical positions of α-W (110) and Mo (110) being equal to 2θ = 40.26° and 2θ = 40.51°, respectively). This shift is linked to the more important amount of Mo in the films deposited at high I_{Mo}. This peak can be attributed to the presence of α-W and/or Mo as the lattice parameters of these two elements are similar with practically identical 2θ values. On the other hand, very weak peaks are detected at nearly the same positions at higher pressure. At low Mo target current, only the β-W phase is weakly detected with (200) and (210) planes at positions 2θ around 35.52° and 39.89°, respectively. At high Mo target current, only the peak corresponding to α-W (110) and/or Mo (110) is marginally pointed out.

W films can adopt two crystallographic structures: the stable phase α-W with a body-centered-cubic (bcc) structure and the metastable β-W phase with a A-15 cubic structure [31-33]. The structural difference between these W phases leads to different lattice parameters, which are equal to a = 0.3165 nm for α-W and a = 0.5040 nm for β-W. The structure of deposited W films and the transformation from β-to-α phase depend on different sputtering parameters as the pressure, deposition rate or temperature [33, 34, 35]. The deposition technique is also one of the important factors that can affect the W crystallography. For example, Karabacak *et al.* [36] reported different crystallographic phases after sputtering deposition performed with normal and oblique incidence of the particle fluxes. With a normal incidence, W films present the two different α and β phases but with a predominance of the α-W phase. In contrast, with

an oblique incidence, the predominance of the β-W phase is noticed. The shadowing effect was proposed to be one of the important factors that can affect the W films crystallography. The defects and the voided structure also influence the W crystallography with an easier incorporation of oxygen favoring the β phase formation [31].

As previously reported, the crystallinity behavior evolves with the sputtering pressure. The quality of W and Mo pure films crystallization strongly decreases with pressure increase [23, 37]. This effect of the sputtering pressure on the films crystallization is also verified for other films as Ti [20], Mo [38], W-W [24]. This poor crystallization is related to the increase of particle interactions with argon atoms during the sputtering until their deposition. At high sputtering pressure, the thermalization degree of the particles increases whereas their energy, mobility and surface diffusion decrease, disturbing the crystallization process and a more disordered structure is produced (also shown in the Supplementary Material). Pure W thin films deposited at low pressure by the GLAD technique are formed with a mixture of α and β phases, the β-W phase being preponderant when two opposite W targets are used [24]. In this last case, an increase of the (200) β-W peak intensity with I_W has also been reported. Furthermore, even if a shift toward higher angles for the (110) peaks with I_{Mo} increase is pointed out, the highest 2θ value ($2\theta = 40.32°$) does not reach the theoretical value for (110) α-Mo equal to 40.51°. A similar behavior has been reported for pure Mo films sputter-deposited at a pressure equal to 0.88 Pa and 1.33 Pa. Chelvanathan *et al.* [37] showed that the (110) peaks were recorded at 2θ values close to 40.2° and 40.5°, respectively.

DC electrical resistivity and electrical anisotropy of W-Mo thin films deposited on glass substrate are measured at room temperature using the van der Pauw method. The role of the sputtering pressure on electrical properties of W-Mo films prepared with various Mo target currents is clearly shown in Figure 7.

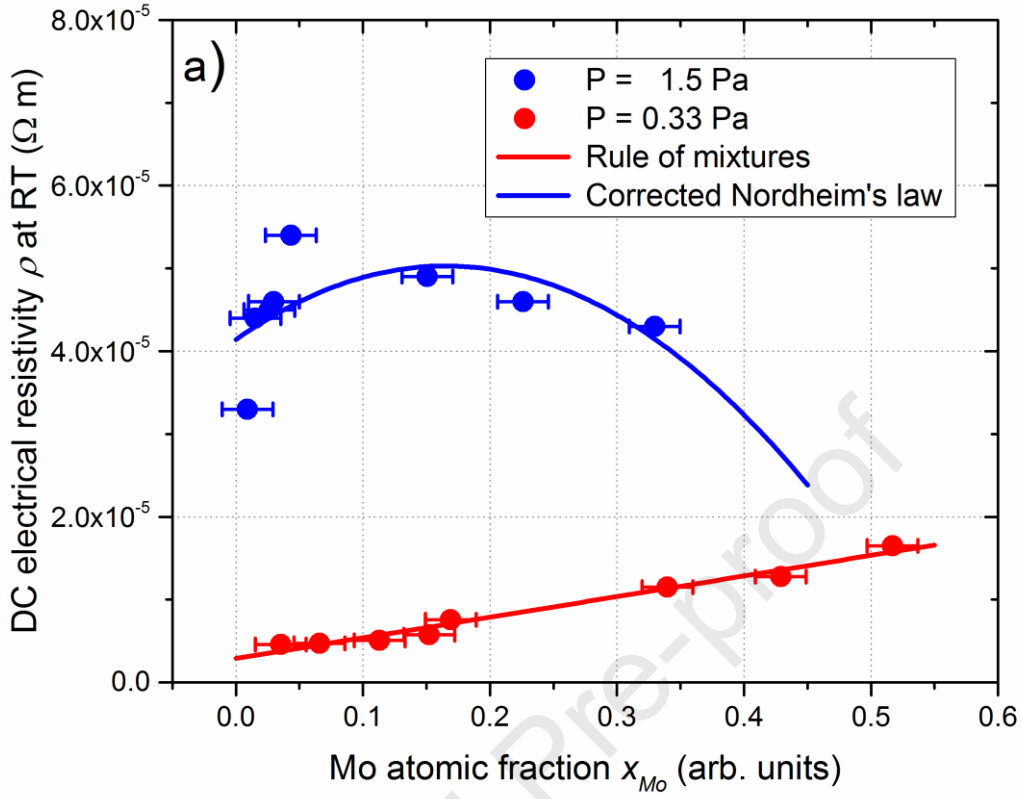

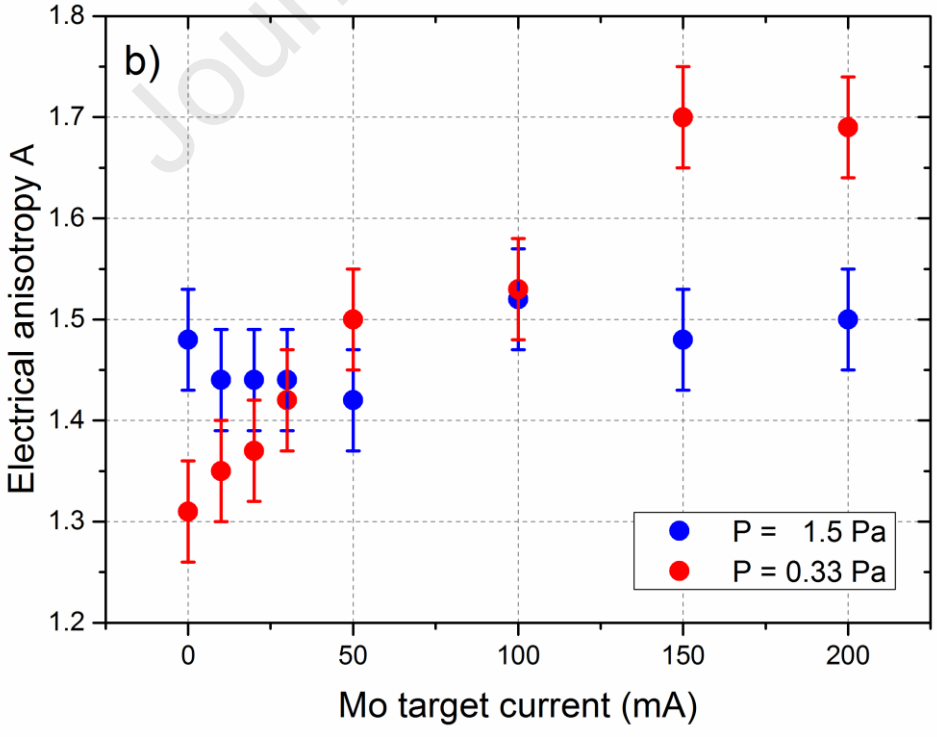

Figure 7: a) DC electrical resistivity at room temperature *vs.* Mo atomic fraction. The rule of mixtures fits at low pressure (red line), whereas a corrected Nordheim's law is applied at high pressure (blue line). b) Electrical anisotropy at room temperature for W-Mo thin films prepared with various Mo target currents and for two different sputtering pressures: 0.33 and 1.5 Pa.

All films present resistivity values 2 to 3 orders of magnitude higher than W and Mo bulk ones (for bulk materials, $\rho_W = 5.39\times10^{-8}$ Ωm and $\rho_{Mo} = 5.47\times10^{-8}$ Ωm at room temperature [39]). These high resistivities are related to GLAD thin film properties that systematically show a high porosity for glancing angle of depositions. The voided structure in these films generate an important electron scattering phenomenon that reduces the carrier mean free path and thus the conducting properties [40].

For films deposited at low pressure, the electrical resistivity ρ exhibits a linear evolution *vs.* Mo atomic fraction (as well as Mo target current). It increases from $\rho = 4.60\times10^{-6}$ Ωm for the lowest Mo concentration (i.e., I_{Mo} = 10 mA) to 1.65×10^{-5} Ωm for the Mo-rich W-Mo films (i.e., I_{Mo} = 200 mA). A similar linear evolution has ever been reported by Jun *et al.* for W-Mo films sputter-deposited with two tilted W and Mo sources [41]. They also stated a gradual evolution of resistivity as a function of the W atomic fraction in biased W-Mo films, but with a reverse trend (i.e., an increase of resistivity for W-rich films). For films prepared with bias, they suggested an enhanced surface mobility of species impinging on the growing film and thus, a more ordered structure. This decreases electron scattering and lowers electrical resistivity. For our W-Mo GLAD films prepared at 0.33 Pa, XRD patterns showed an increased intensity of diffracted signals corresponding to the β-W phase (Fig. 6). Since the latter is more resistive than the α-W phase ($\rho_{\beta\text{-}W} = 1.5\text{-}3.5\times10^{-6}$ Ωm, whereas $\rho_{\alpha\text{-}W} = 5.39\times10^{-8}$ Ωm at room temperature [39, 42]) one can expect more resistive W-Mo films as Mo concentration rises. In

addition, oblique angle deposition favors growing defects in the columnar structure, which reduces the electron mean free path and favors less conductive films.

Our results in Fig. 7a) do not follow the Nordheim's law [41], but rather a rule of mixtures. At first, we can assume this rule of mixtures following:

$$\rho = \rho_T + \rho_R + x_{Mo} \times \rho_{Mo} + x_W \times \rho_W \quad (5)$$

where ρ_T is the resistivity due to electron-phonon interactions (Ωm), ρ_R the resistivity due to the electron scattering by crystal defects (Ωm), x_{Mo} and x_W the Mo and W atomic fractions (arb. units), respectively, and ρ_{Mo} and ρ_W the resistivity of Mo and W, respectively. Neglecting first ρ_T and ρ_R compared to ρ_{Mo} and ρ_W at room temperature, the linear interpolation of ρ *vs.* x_{Mo} gives rise to $\rho_{Mo} = 2.78\times10^{-5}$ Ωm and $\rho_W = 2.90\times10^{-6}$ Ωm with a good agreement between fitting according to a rule of mixtures and experimental data (Fig. 7a). Again, resistivity values of Mo and W are several orders of magnitude higher than that of bulk materials, which is related to the porous character and the large concentration of defects of W-Mo GLAD films.

For samples prepared at high pressure, the measured electrical resistivity values are systematically higher than those obtained at low pressure. It is mainly assigned to the disordered structure (weak diffracted signal from XRD in Fig. 6) as well as to the smaller size of the columns with a cauliflower morphology (SEM observations in Fig. 3 and 4). In addition, ρ *vs.* x_{Mo} exhibits a maximum of electrical resistivity with $\rho > 5\times10^{-5}$ Ωm for x_{Mo} close to 0.1-0.2 (corresponding to I_{Mo} = 50 mA). Jun *et al.* also measured such a maximum for unbiased W-Mo films for W atomic fraction around 0.5 [41]. This behavior is typical of some binary metallic alloys following the Nordheim's rule, where electron scattering originates from solute atoms, second phase, grain boundaries, defects and impurities. For our W-Mo GLAD films prepared at high pressure, the highest resistivity is far from an atomic fraction of 0.5, and thus, a corrected Nordheim's law is rather suggested following [43, 44]:

$$\rho = \rho_0 + C \times x_{Mo}(1 - D \times x_{Mo}) \quad (6)$$

Where ρ_0 combines resistivity due to electron-phonon interactions and electron scattering by crystal defects (Ωm), C the Nordheim coefficient (Ωm) and D is a constant (in (atomic fraction)$^{-1}$).

From resistivity measurements and atomic concentration ratio *vs.* Mo target current (Fig. 5), interpolation gives $\rho_0 = 4.14\times10^{-5}$ Ωm, $C = 1.08\times10^{-5}$ Ωm and $D = 3.03$. Nordheim coefficient and ρ_0 value are both about 3 orders of magnitude higher than that of bulk alloys, which could be expected in GLAD films due to defects and porous structure. About the quantity D, it is worth noting that resistivity of bulk alloys in accordance with the corrected Nordheim's law shows D values of a few (atomic ratio)$^{-1}$. W-Mo GLAD films prepared at high pressure do not exhibit neither a well-defined crystal structure from XRD patterns (Fig. 6), nor a clear microstructure but rather a randomized columnar and cauliflower morphology from SEM pictures (Fig. 3b and 4b). However, W and Mo atoms are not completely and randomly located in the columns since D value higher than 1 may suggest clustering or short-range order effect [44].

The electrical anisotropy A is defined as the ratio between electrical resistivity measured in the direction parallel ($\rho_{//}$) and perpendicular ($\rho_{\perp}$) to the particle fluxes. The electrical anisotropy *vs.* Mo target current presents different behaviors at low and high pressures as shown in Fig. 7b. At low pressure, it significantly increases from $A = 1.3$ for $I_{Mo} = 10$ mA to $A = 1.7$ as I_{Mo} reaches 200 mA while it presents nearly constant values in-between 1.4-1.5 at high pressure. The electrical anisotropy behavior is mainly linked to the thin film morphology. At low pressure, A is related to the elliptical form of the columns as reported in SEM observations. This enhanced anisotropy with Mo target current correlates with the highest Mo particle flux that leads to a more important lateral growth, a more elongated columns shape and therefore a more elliptic form. At high pressure, the nearly constant electrical anisotropy is assigned to the

unchangeable cauliflower microstructure whatever the Mo target current applied for the film deposition.

Conclusion

The GLAD co-sputtering technique implementing two separated W and Mo targets is developed to prepare W-Mo thin films using the same oblique angle of deposition (α = 80°). A systematic change of the Mo target current intensity is carried out (from 10 to 200 mA), whereas the W target is sputtered with a constant current of 140 mA. Two argon sputtering pressures are applied: 0.33 Pa (low pressure) and 1.5 Pa (high pressure) corresponding to ballistic and thermalized regimes of sputtered particles, respectively.

Films exhibit a porous and columnar structure with more or less slanted columnar architecture. Tilting of the columns can be adjusted playing with these two key parameters: Mo target current and sputtering pressure. At low sputtering pressure, W-Mo thin films exhibit elliptic forms of the column cross-section and the predominance of the β-W phase. These structural features are mainly assigned to the ballistic character of W and Mo sputtered atoms. A more isotropic shape of the column section (cauliflower microstructure and bundling phenomenon of the columns) with a poorly crystalline structure is produced at high pressure. This is due to the mainly thermalized regime of W and Mo atoms corresponding to less directional fluxes of sputtered particles impinging on the growing film.

The electrical resistivity and anisotropy both show different behaviors at low and high pressures as a function of the Mo target current and so Mo content in the films. Resistivity of W-Mo films prepared at low pressure rather follows a rule of mixtures as the Mo concentration increases with a enhanced anisotropy. The highest resistivity is systematically obtained at high pressure for any Mo content with a good agreement with a corrected Nordheim's law (maximum of resistivity is shifted to W-rich films).

These results show that ballistic and thermalized regimes are easily tuned by means of the working pressure and depend on the nature of sputtered atoms. These regimes lead to two opposite operating conditions and allow tuning microstructure and morphology of GLAD co-

sputter-deposited binary films. Resulting film properties, especially electrical resistivity can be largely adjusted, which extend the range of conductive thin films for device applications.

CRediT authorship contribution statement

Houssem Boukhalfa: Data curation, writing – original draft. **Valérie Potin:** Writing - review & editing, Supervision, Funding acquisition. **Nicolas Martin:** Writing - review & editing, Supervision, Funding acquisition

Declaration of Competing Interest

The authors declare that they have no known competing financial interests or personal relationships that could have appeared to influence the work reported in this paper.

Acknowledgement

This work has been supported by the Region Bourgogne Franche-Comté and by EIPHI Graduate School (Contract 'ANR-17-EURE-0002').

Appendix A. Supplementary data

Supplementary data to this article can be found on line at https://doi. …

References

[1] J.E. Greene, Tracing the 5000-year recorded history of inorganic thin films from similar to 3000 BC to the early 1900s AD, Appl. Phys. Rev. 1 (2014) 041302-041337. http://dx.doi.org/10.1063/1.4902760

[2] M. Beshkova, L. Hutlman, Yakimova, Device applications of epitaxial graphene on silicon carbide, Vacuum, 128 (2016) 186-197. https://doi.org/10.1016/j.vacuum.2016.03.027

[3] A. Rydosz, K. Dyndal, K. Kollbek, W. Andrysiewicz, M. Sitarz, K. Marszalek, Structure and optical properties of the WO3 thin films deposited by the GLAD magnetron sputtering technique, Vacuum, 177 (2020) 109378-9. https://doi.org/10.1016/j.vacuum.2020.109378

[4] M.J. Brett, M.T. Taschuk, Matthew M. Hawkeye, Glancing Angle Deposition of Thin Films, John Wiley & Sons, Ltd, Chichester, 2014. https://doi.org/10.1002/9781118847510

[5] M.T. Taschuk, M.M. Hawkeye, M.J. Brett, Glancing Angle Deposition, in: P.M. Martin (Ed.), Handbook of deposition Technologies for films and coatings, 3rd Edition, Elsevier, Oxford, 2010, pp 621-678. https://doi.org/10.1016/b978-0-8155-2031-3.00013-2

[6] C.M. Zhou, H.F. Li and D. Gall, Multi-component nanostructure design by atomic shadowing, Thin Solid Films 517 (2008) 1214-1218. http://dx.doi.org/10.1016/j.tsf.2008.05.049

[7] C.M. Zhou and D. Gall, Two-Component Nanorod Arrays by Glancing-Angle Deposition, Small, 4(9) (2008) 1351-1354. https://doi.org/10.1002/smll.200701289

[8] R. El Beainou, N. Martin, V. Potin, P. Pedrosa, M. Arab Pour Yazdi, A. Billard, Correlation between structure and electrical resistivity of W-Cu thin films prepared by GLAD co-sputtering, Surf. Coat. Technol. 313 (2017) 1-7. http://dx.doi.org/10.1016/j.surfcoat.2017.01.039

[9] H. Boukhalfa, V. Potin, N. Martin, Microstructural analysis and electrical behaviours of co-sputtered W–Ag thin films with a tilted columnar architecture, J. Phys. D: Appl. Phys. 54 (2021) 255304-255312. https://doi.org/10.1088/1361-6463/abf312

[10] P. Pedrosa, A. Ferreira, N. Martin, M. Arab Pour Yazdi, A. Billard, S. Lanceros-Méndez, F. Vaz, Nano-sculptured Janus-like TiAg thin films obliquely deposited by GLAD co-sputtering for temperature sensing, Nanotechnology 29 (2018) 355706-11. https://doi.org/10.1088/1361-6528/aacba8

[11] C. Jetjamnong, S. Chatikaprakhan, R. Kowong, C. Chananonnawathorn, A. Bootchanont, T. Lertvanithphol, S. Limwichean, P. Kijamnajsuk, A. Klamchuen, G. Meng, A. Watcharapasorn, H. Nakajima, M. Horprathum, Growth and characterization of NiWO nanorod films prepared by reactive magnetron co-sputtering with oblique angle deposition, Vacuum, 196 (2022) 110777-8. https://doi.org/10.1016/j.vacuum.2021.110777

[12] R. El Beainou, N. Martin, V. Potin, P. Pedrosa, M. Arab Pour Yazdi, A. Billard, W-Cu sputtered thin films grown at oblique angles from two sources: Pressure and shielding effects, Surf. Coat. Technol. 343 (2017) 153-159. https://doi.org/10.1016/j.surfcoat.2017.09.062

[13] J.M. García-Martín, R. Alvarez, P. Romero-Gómez, A. Cebollada, A. Palmero, Tilt angle control of nanocolumns grown by glancing angle sputtering at variable argon pressures, Appl. Phys. Lett. 97 (2010) 173103-173105. https://doi.org/10.1063/1.3506502

[14] R. Alvarez, J.M. Garcia-Martin, M.C. Lopez-Santos, V. Rico, F.J. Ferrer, J. Cotrino, A.R. Gonzalez-Elipe, A. Palmero, On the Deposition Rates of Magnetron Sputtered Thin Films at Oblique Angles, Plasma Process. Polym. 11(6) (2014) 571-576. https://doi.org/10.1002/ppap.201300201

[15] A. Garcia-Valenzuela, R. Alvarez, V. Rico, J. Cotrino, A.R. Gonzalez-Elipe, A. Palmero, Growth of nanocolumnar porous TiO_2 thin films by magnetron sputtering using particle

collimators, Surf. Coat. Technol. 343 **(**2018**)** 172-177. https://doi.org/10.1016/j.surfcoat.2017.09.039

[16] R. El Beainou, A. Chargui, P. Pedrosa, A. Mosset, S. Euphrasie, P. Vairac, N. Martin, Electrical resistivity and elastic wave propagation anisotropy in glancing angle deposited tungsten and gold thin films, Appl. Surf. Sci. 475 (2019) 606-614. https://doi.org/10.1016/j.apsusc.2019.01.041

[17] M. Rausch, M. Pavlovič, P. Kreiml, M.J. Cordill, J. Winkler, C. Mitterer, Sputter deposition of Mo-based multicomponent thin films from rotatable targets: experiment and simulation, Appl. Surf. Sci. 455 (2018) 1029-1036. https://doi.org/10.1016/j.apsusc.2018.06.012

[18] O. Bierwagen, R. Pomraenke, S. Eilers, W.T. Masselink, Mobility and carrier density in materials with anisotropic conductivity revealed by van der Pauw measurements, Phys. Rev. B 70 (2004) 165307-165312. https://doi.org/10.1103/PhysRevB.70.165307

[19] W.D. Westwood, Calculation of deposition rates in diode sputtering systems, J. Vac. Sci. technol. 15(1) (1978) 1-9. https://doi.org/10.1116/1.569429

[20] P. Pedrosa, A. Ferreira, J.M. Cote, N. Martin, M. Arab Pour Yazdi, A. Billard, S. Lanceros-Mendez, F. Vaz, Influence of the sputtering pressure on the morphological features and electrical resistivity anisotropy of nanostructured titanium films, Appl. Surf. Sci. 420 (2017) 681-690. https://doi.org/10.1016/j.apsusc.2017.05.175

[21] C.R.D. Priestland, S.D. Hersee, The effects of pressure on the deposition rate in rf sputtering processes, Vacuum 22(3) (1972) 103-106. https://doi.org/10.1016/0042-207x(72)90468-x

[22] D.O. Smith, M.S. Cohen, G.P. Weiss, Oblique-Incidence Anisotropy in Evaporated Permalloy Films, J. Appl. Phys. 31 (1960) 1755-1762. https://doi.org/10.1063/1.1735441

[23] A. Barranco, A. Borras, A.R. Gonzalez-Elipe, A. Palmero, Perspectives on oblique angle deposition of thin films: From fundamentals to devices, Prog. Mater. Sci. 76 (2016) 59-153. http://dx.doi.org/10.1016/j.pmatsci.2015.06.003

[24] V. Potin, H. Boukhalfa, N. Martin, Oblique angle co-deposition of nanocolumnar tungsten thin films with two W sources: Effect of pressure and target current, Mater. Chem. Phys., 281 (2022), 125864-11. https://doi.org/10.1016/j.matchemphys.2022.125864

[25] A. Chargui, R. El Beainou, A. Mosset, S. Euphrasie, V. Potin, P. Vairac, N. Martin, Influence of Thickness and Sputtering Pressure on Electrical Resistivity and Elastic Wave Propagation in Oriented Columnar Tungsten Thin Films, Nanomaterials 10 (2020) 81-99. https://doi.org/10.3390/nano10010081

[26] R. Krishnan, M. Riley, S. Lee, T.M. Lu, Vertically aligned biaxially textured molybdenum thin films, J. Appl. Phys. 110 (2011) 064311-064316. https://doi.org/10.1063/1.3638452

[27] R. El Beainou, J.M. Cote, V. Tissot, V. Potin, N. Martin, Resistivity anisotropy of tilted columnar W and W-Cu thin films, Surf. Coat. Technol., 421 (2021) 127412-11. https://doi.org/10.1016/j.surfcoat.2021.127412

[28] R. Alvarez, J.M. Garcia-Martin, A. Garcia-Valenzuela, M. Macias-Montero, F.J. Ferrer, J. Santiso, V. Rico, J. Cotrino, A.R. Gonzalez-Elipe, A. Palmero, Nanostructured Ti thin films by magnetron sputtering at oblique angles, J. Phys. D: Appl. Phys. 49 (2016) 045303-045312. https://doi.org/10.1088/0022-3727/49/4/045303

[29] P. Solar, A. Choukourov, J. Hanus, E. Pavlova, D. Slavinska, H. Biederman, Nanocomposite structured thin films by magnetron sputtering at glancing angle deposition, Proceedings of the International Plasma Chemistry Society, Bochum, Germany 27-31 (2009) 226.

[30] S.Y. Davydov, Calculation of the activation energy for surface self-diffusion of transition-metal atoms, Phys. Solid State 41 (1999) 8-10. https://doi.org/10.1134/1.1130717

[31] M.J. O'Keefe, J.T. Grant, Phase transformation of sputter deposited tungsten thin films with A15 structure, J. Appl. Phys. 79 (1996) 9134-9141. http://dx.doi.org/10.1063/1.362584

[32] L. Chen, T.M. Lu, G.C. Wang, Creation of biaxial body center cubic tungsten nanorods under dynamic shadowing effect, Thin Solid Films 539 (2013) 65-69. https://doi.org/10.1016/j.tsf.2013.04.151

[33] S.M. Rossnagel, I.C. Noyan, C. Cabral Jr., The Phase Transformation of Thin Sputter-deposited Tungsten Films at Room Temperature, J. Vac. Sci. Technol. B 20 (2002) 2047-2051. http://dx.doi.org/10.1116/1.1506905

[34] F.T.N. Vüllers, R. Spolenak, Alpha- vs. beta-W nanocrystalline thin films: A comprehensive study of sputter parameters and resulting materials properties, Thin Solid Films 577 (2015) 26-34. http://dx.doi.org/10.1016/j.tsf.2015.01.030

[35] K. Barmak, J. Liu, Impact of deposition rate, underlayers, and substrates on β−tungsten formation in sputter deposited films, J. Vac. Sci. Technol. A 35 (2017) 061516. https://doi.org/10.1116/1.5003628

[36] T. Karabacak, A. Mallikarjunan, J.P. Singh, D. Ye, G.C. Wang, T.M. Lu, β-phase tungsten nanorod formation by oblique-angle sputter deposition, Appl. Phys. Lett. 83 (2003) 3096-3098. https://doi.org/10.1063/1.1618944

[37] P. Chelvanathan, S.A. Shahahmadi, F. Arith, K. Sobayel, M. Aktharuzzaman, K. Sopian, F.H. Alharbi, N. Tabet, N. Amin, Effects of RF magnetron sputtering deposition process parameters on the properties of molybdenum thin films, Thin Solid Films, 638 (2017) 213-219. https://doi.org/10.1016/j.tsf.2017.07.057

[38] G. Zoppi, N.S. Beattie, J.D. Major, R.W. Miles, I. Forbes, Electrical, morphological and structural properties of RF magnetron sputtered Mo thin films for application in thin film photovoltaic solar cells, J Mater Sci 46 (2011) 4913-4921. https://doi.org/10.1007/s10853-011-5404-0

[39] D.R. Lide, CRC Handbook of Chemistry and Physics, Internet Version 2005, CRC Press, FL, Boca Raton, 2005

[40] A. Besnard, N. Martin, L. Carpentier, B. Gallas, A theoretical model for the electrical properties of chromium thin films sputter deposited at oblique incidence, J. Phys. D 44 (2011) 215301-215308. https://doi.org/10.1088/0022-3727/44/21/215301

[41] S.I. Jun, P.D. Rack, T.E. McKnight, A.V. Melechko, M.L. Simpson, Electrical and microstructural characterization of molybdenum tungsten electrodes using combinatorial thin film sputtering technique, J. Appl. Phys., 97 (2005) 054906-6. https://doi.org/10.1063/1.1855395

[42] D. Choi, B. Wang, S. Chung, X. Liu, A. Darbal, A. Wise, N.T. Nuhfer, K. Barmak, Phase, grain structure, stress, and resistivity of sputter-deposited tungsten films, J. Vac. Sci. Technol., A29(5) (2011) 051512-8 https://doi.org/10.1116/1.3622619.

[43] S.Y. Komatsu, M. Ikeda, T. Kohmoto, H. Yukimachi, Corrected Nordheim's law for aluminum base high concentration solid solutions, Proceedings of ICAA-6, 2 (1998) 867-872.

[44] J.O. Linde, An experimental study of resistivity-concentration dependence of alloys, Helv. Phys. Acta, 41 (1968) 1007-1015.

Declaration of interests

☒ The authors declare that they have no known competing financial interests or personal relationships that could have appeared to influence the work reported in this paper.

☐ The authors declare the following financial interests/personal relationships which may be considered as potential competing interests: